

Direct Deoxydehydration of Cyclic *trans*-Diol Substrates: An Experimental and Computational Study of the Reaction Mechanism of Vanadium(V)-based Catalysis**

Ebru Aksanoglu,^[a, b] Yee Hwee Lim,^{*, [b]} and Richard A. Bryce^{*, [a]}

The deoxydehydration of carbohydrates represents a key target to leverage renewable biomass resources chemically. Using a vanadium(V)-based catalyst, it was possible to directly deoxydehydrate cyclic *trans*-diol substrates. Accompanying mechanistic characterisation of this process by density functional calculations pointed to an energetically tractable route for deoxydehydration of cyclic *trans*-diol substrates involving

stepwise cleavage of the diol C–O bonds via the triplet state; experimentally, this was supported by light dependence of the reaction. Calculations also indicated that cyclic *cis*-diols and a linear diol substrate could additionally proceed by a concerted singlet DODH mechanism. This work potentially opens a new and cost-effective way to efficiently convert carbohydrates of *trans*-diol stereochemistry into alkenes.

Introduction

With the rapid depletion of fossil fuel resources, there is an urgency to leverage biomass for high-value chemicals as a replacement for petrochemical-based products, from fuels, dispersants and detergents, to rheology modifiers and flocculants.^[1] Carbohydrates such as cellulose and starch constitute the largest source of biomass substrate. However, the synthesis and selective modification of saccharides is challenging. Enzymatic modification approaches show promise but face significant challenges in terms of titre yield, process accessibility and eventual industry applicability, often requiring further chemical or physical processing.^[2]

Carbohydrate conversion using selective non-enzymatic catalysis has also received considerable attention. Characterised by the large number of hydroxyl groups in carbohydrate systems, most modifications are restricted to acetylation and esterification, to crosslink or incorporate additional functionalities. To improve the value of carbohydrates as chemical precursors, it is desirable to reduce their oxygen content;

unfortunately, there are relatively few reactions known to be successful for reducing the oxygen content of biomass-derived polyols.^[3] The most widely employed deoxygenation reactions are acid-catalysed dehydration, high-temperature pyrolysis and hydrogenolysis. However, hydrodeoxygenation and deoxydehydration (DODH) reactions have become increasingly used, producing alkanes and alkenes, respectively.^[4] The formation of alkenes as opposed to alkanes is advantageous to the chemical industry, as the olefin functional group can be further manipulated via addition reactions and oligomerisation to yield polymeric materials.^[5]

DODH reactions convert diols to alkenes (Figure 1) and generally require a metal catalyst, a reductant and a solvent.^[6] Metal catalysts that have been successfully explored are rhenium,^[7] vanadium^[8] and molybdenum.^[9] Rhenium has provided the most efficient and highest yielding catalysts but is the most expensive of the three metals. The substrate scope of the reaction includes simple aliphatic diols, cyclic diols and more recently, sugar alcohols containing many vicinal diol moieties.^[7f] In general, it is observed experimentally for rhenium-catalysed DODH reactions that (i) terminal diols undergo DODH faster

[a] E. Aksanoglu, Dr. R. A. Bryce
Division of Pharmacy and Optometry, School of Health Sciences
Manchester Academic Health Sciences Centre
University of Manchester
Oxford Road, Manchester M13 9PL (UK)
E-mail: R.A.Bryce@manchester.ac.uk

[b] E. Aksanoglu, Dr. Y. H. Lim
Functional Molecules & Polymers
Institute of Chemical and Engineering Sciences
8 Biomedical Grove, #07-01/02, Singapore 138665 (Singapore)
E-mail: lim_yee_hwee@ices.a-star.edu.sg

[**] A previous version of this manuscript has been deposited on a preprint server (<https://doi.org/10.26434/chemrxiv.13140428.v1>).

Supporting information for this article is available on the WWW under <https://doi.org/10.1002/cssc.202002594>

© 2021 The Authors. ChemSusChem published by Wiley-VCH GmbH. This is an open access article under the terms of the Creative Commons Attribution Non-Commercial NoDerivs License, which permits use and distribution in any medium, provided the original work is properly cited, the use is non-commercial and no modifications or adaptations are made.

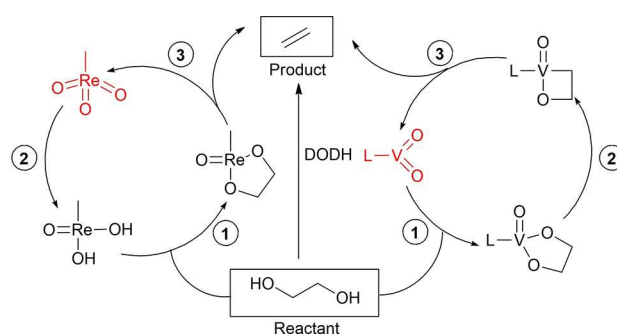


Figure 1. Rhenium-catalysed (left) and vanadium-catalysed (right) DODH reactions of ethylene glycol. Steps 1, 2 and 3 refer to condensation of the diol, reduction and olefin-extrusion, respectively. Catalysts are shown in red.

than internal diols;^[10] and (ii) cyclic *cis*-diols are able to undergo DODH reactions whereas cyclic *trans*-diols cannot.^[7c,k,11]

As an example of (ii), Abu-Omar and co-workers reported a cyclohexene yield of 60% when *cis*-1,2-cyclohexanediol underwent methyltrioxorhenium (MTO)-catalysed DODH using hydrogen as the reductant.^[7b] However, the *trans* isomer did not undergo DODH. Shiramizu and Toste reported the MTO-catalysed DODH reaction of cyclic sugars, some of which contained *trans*-diol moieties.^[7f] The findings supported the preference for the *cis* stereochemistry; however, the *trans*-diol sugars did react, albeit providing low alkene yields. Speculation as to the underlying mechanism of this cyclic *trans*-diol DODH included pyranose ring opening to provide an acyclic substrate capable of the *syn* stereochemistry for olefin extrusion.^[7f] While *cis*-DODH is suited to sugars such as D-mannose, this is unfortunate for *trans*-diol substrates including the key biomass residue, D-glucose.

Insight into the inability of MTO to process *trans*-cyclic diol substrates was provided by quantum chemical calculation of the DODH reaction mechanism by Wang and co-workers.^[12] This density functional theory (DFT) study compared DODH of *trans*- and *cis*-1,4-anhydroerythritol (denoted here as **S1** and **S1'** respectively, Figure S1a) using the M06/SDD/6-311++G** level of theory and a continuum model for the 3-octanol solvent. Using this model, the key olefin extrusion barrier energy for the *trans*-diol **S1** substrate was found to be 50 kcal mol⁻¹ higher than the 19.9 kcal mol⁻¹ barrier for the *cis* isomer **S1'**. The substantial difference in barrier height was attributed to the stereospecific requirements of the retrocycloaddition reaction: the concerted olefin extrusion transition state was formed with the requirement for a *syn* approach of the diol's OH groups to the Re centre. Here, due to its diol stereochemistry, the cyclic *trans*-diol could not adopt the planar arrangement in the concerted breakage of both Re–O bonds between the catalyst and the diol, required for a low energy barrier to this extrusion step (Figure S1b).

As an alternative to rhenium-based DODH, recent work has demonstrated the ability of homogeneous vanadium complexes to catalyse DODH of vicinal diols in comparable yields.^[8] An example is the DODH of 1,2-propanediol to form propene, using [*n*-Bu₄N]-(dipic)VO₂ catalyst **1**, triphenylphosphine as the reductant and benzene as the solvent. For this reaction, computational work by Jiang et al.^[13] and Poutas et al.^[14] reported novel spin-crossover mechanisms. The spin-crossover, involving vanadium's triplet state, provided a lower energy path than a previously proposed one-step olefin extrusion mechanism.^[15] In the proposed crossover mechanisms, the key olefin-extrusion step occurs stepwise rather than via concerted cleavage of the diol C–O bonds required by MTO-catalysed DODH (Figures 1 and 2).

In this study, we explore the possibility that the preferred stepwise catalytic route exploited by vanadium catalysts could allow sufficient flexibility for DODH of a cyclic diol of *trans* stereochemistry (Figure 2). Vanadium DODH has been shown to occur for a cyclic substrate of *cis*-stereochemistry: specifically, it was reported that [*n*-Bu₄N]-(dipic)VO₂ catalysed the DODH of *cis*-1,2-cyclohexanediol, producing a cyclohexene yield of

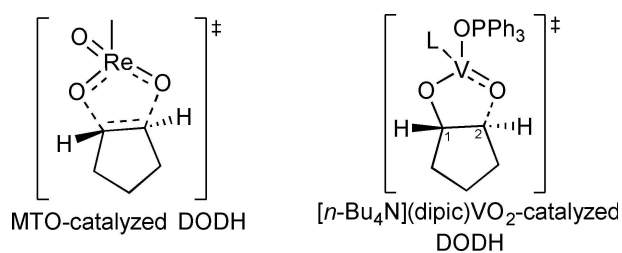


Figure 2. Comparison of (left) rhenium-catalysed DODH key olefin-extrusion transition state, where C–O cleavage is concerted; and (right) vanadium-catalysed DODH key olefin-extrusion transition state, where C–O cleavage is stepwise. Numbering of diol C–O atoms indicated.

15%.^[8a] However, to our knowledge, vanadium-catalysed DODH of cyclic *trans*-diol substrates remains unexplored. Indeed, prior mechanistic studies on the vanadium-catalysed DODH of vicinal diols have focused on model linear substrates with no exploration of the *cis* or *trans* preference of cyclic diol substrates. Therefore, in this work we investigate by experiment and computation the ability of vanadium(V) species to catalyse the DODH reaction of cyclic *trans*-diols and compare with their *cis* isomers.

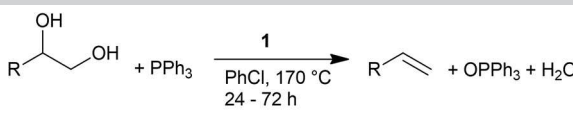
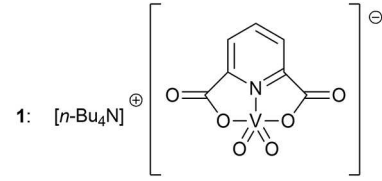
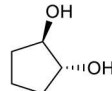
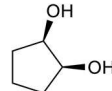
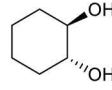
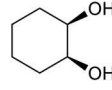
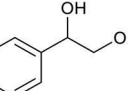
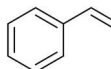
Results and Discussion

Cyclic *trans*-diol substrates can undergo direct DODH

To confirm our hypothesis, first we investigate whether [*n*-Bu₄N]-(dipic)VO₂ **1** is able to catalyse the DODH of *trans*-1,2-cyclopentanediol (**S2**) and compare with its *cis* isomer (**S2'**) (Table 1). 10 mol% of **1** was used, in chlorobenzene, with triphenylphosphine as the reductant. We find that **S2** gives a cyclopentene yield of 20%, and that this is 2% higher than that of its *cis*-isomer **S2'** (Table 1). Similarly, we see comparable yields for *cis* and *trans* isomers for a substrate with a six-membered ring: *trans*-1,2-cyclohexanediol **S3** gives a cyclohexene yield of 14%, in comparison to 16% for its *cis*-isomer **S3'** (Table 1). As a further comparison, we carried out DODH of 1-phenyl-1,2-ethanediol **S4** (styrenediol, Table 1), a linear substrate that is widely used as substrate for DODH reactions. **S4** is able to undergo DODH efficiently to give the olefin product, styrene, due to the driving force of generating a product with extended conjugation. Here, we report a styrene yield from **S4** of 36% (Table 1). Given the lack of conversion for cyclic *trans*-diol substrates via rhenium-catalysed DODH, the reactivity of *trans*-diol substrates **S2** and **S3** observed here using a vanadium-based catalyst is notable, as is the approximate parity in yield with their *cis*-isomers.

As mentioned above, preceding computational work^[13] suggested the involvement of a spin-crossover mechanism in vanadium-catalysed DODH. Specifically, Jiang et al. predict that the [*n*-Bu₄N]-(dipic)VO₂-catalysed DODH reaction proceeds via intersystem crossings (ISC) involving singlet and triplet states.^[13] A DFT study by Poutas et al. described a variant of this mechanism, also utilising vanadium's triplet state.^[14] Both of

Table 1. Oxo-vanadium catalysed DODH of substrates in normal light and dark conditions.^[a]

Substrate	Product	Yield [%] light ^[b]	dark ^[c]	Fold Δ ^[d]
				
				
		20	6	3.3
		18	4	4.5
		14	6	2.3
		16	3	5.3
		36	14	2.6

[a] Reaction conditions: 0.1 mmol substrate, 0.15 mmol PPh₃, and 10 mol% of the catalyst. Reaction time is 72 h unless otherwise stated. Yields are determined by ¹H NMR spectroscopy using mesitylene as the internal standard and based on an average of three repeats. [b] Olefin yield when the reaction was carried out in normal light. [c] Olefin yield in the dark. [d] Fold difference (fold Δ) is calculated as (yield in light)/(yield in dark). [e] Reaction time is 24 h.

these stepwise mechanisms have a lower computed energy pathway than a previously proposed concerted route.^[15]

Therefore, given the potential involvement of ISC events, we carried out the reaction in the presence and absence of visible light, in order to identify any role for photocatalysis in this reaction. As borosilicate glassware was used for this reaction, the effects of UV radiation were precluded. When DODH was performed for the 1,2-cyclopentanediols **S2** and **S2'**, 1,2-cyclohexanediols **S3** and **S3'** and styrenediol **S4** under these conditions, we do indeed find that light has a significant effect on this reaction, with enhancements in yield ranging from 2.3-fold to 5.3-fold (Table 1). We observe that the disparity in yield was most pronounced for the *cis*-cyclic diols **S2'** and **S3'**, where the presence of light increases the yield 4.5- and 5.3-fold, respectively. Although ISC events can be thermally activated in some instances, we observe here that the presence of light

results in enhanced yields of olefin products. Thus, we propose that the role of light in this reaction is providing additional energy for this ISC event to take place. However, the absence of light does not completely halt the reaction; this may indicate the presence of alternative routes to one involving ISC, such that when light is excluded, the reaction proceeds via less favourable singlet pathways. This may also hint that thermal activation is suitable for this ISC event to take place, but at a significantly lower efficiency.

Mechanistic insights from density functional calculations

To further investigate the mechanistic basis of our observed DODH reactions and their light dependence, using DFT we compute the free energy surfaces of vanadium-catalysed DODH of cyclic *trans*- and *cis*-diols, and compare with the energetics for the linear substrate, 1-phenyl-1,2-ethanediol **S4**.

The previously proposed^[13] spin-crossover mechanism of vanadium-catalysed DODH of vicinal diols to alkenes involves six steps: (a) condensation of the diol onto the vanadium catalyst; (b) reduction of the vanadium-diolate from its (V) to (III) state; (c) crossover from the singlet to triplet state of vanadium; (d) scission of one of the diol C–O bonds, forming a carbon-centred radical on the resulting vanadium(IV) species; (e) a second spin-crossover to form a vanadium metallacycle in the singlet state and finally, (f) concerted C–O and C–V bond cleavage to form the alkene product and regenerate the catalyst in its starting singlet state. Thus, the olefin extrusion stage comprises steps (c) to (f).

Five-membered ring substrates

We first consider the spin-crossover DODH mechanism for the five-membered carbocyclic *trans*-diol substrate **S2** (Figure 3). In step (a), there is condensation of **S2** with the vanadium catalyst **1** (Figure 3); during this, there are two consecutive proton transfers from substrate to catalyst to yield intermediate **5s**; here, two V–O bonds are formed between the substrate diol and the vanadium catalyst. The highest barrier found in step (a) is the second proton transfer and formation of the second V–O bond, which occurs via **TS2 s**, with a calculated free energy of 30.8 kcal mol^{−1} relative to the starting catalyst and substrate diol. Step (b) involves the reduction of the vanadium-diolate intermediate **6s** by triphenylphosphine (Figure 3). Water is first expelled from complex **5s**, exergonically forming complex **6s**. The phosphorus atom of the triphenylphosphine reagent attacks the oxo ligand of **1** and reduces the vanadium complex from a V^V to V^{III} oxidation state, giving the catalytically active form **7s** via **TS3 s**. This barrier is calculated as 40.3 kcal mol^{−1} at the M06-L/SDD/6-311+G**/SMD level of theory. As vanadium (III) complexes possess triplet ground states, intermediate **7s** converts to intermediate **7t** via a minimum-energy crossover point, **MECP1**, in a spin-crossover process (Figure 4); this is in accord with preceding quantum chemical studies for DODH of linear substrates.^[13,14]

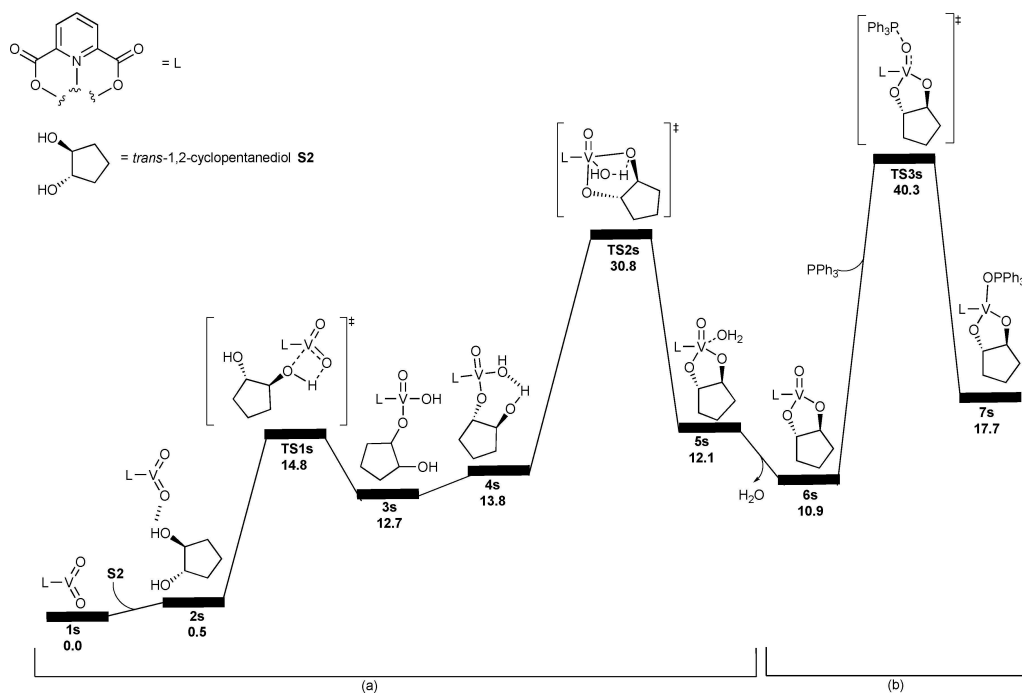


Figure 3. Proposed reaction mechanism for DODH of *trans*-1,2-cyclopentanediol (**S2**), catalysed by **1**, utilising PPh_3 as reductant. Free energies [kcal mol^{-1}] computed at the M06-L/SDD/6-311 + G^{**} /SMD level of theory. Steps (a) and (b) denote condensation of the substrate onto catalyst, and reduction of the metal-diolate species, respectively. For clarity, dipicolinate ligand (inset) is defined as L. Also note that vanadium dipicolinate complexes have a net charge of -1 .

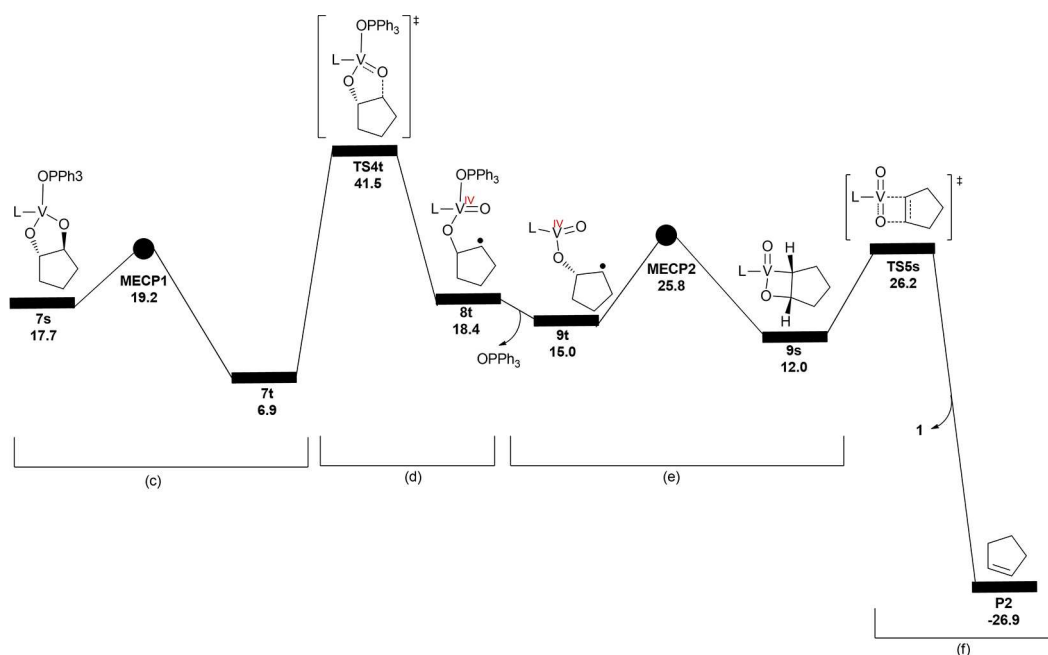


Figure 4. Proposed reaction mechanism for DODH of **S2**, showing steps (c–f). Free energies [kcal mol^{-1}] computed at the M06-L/SDD/6-311 + G^{**} /SMD level of theory.

Potentially the order of condensation [step (a)] and reduction [step (b)] could be reversed as pointed out by Poutas et al.^[14] Considering the possibility of reduction preceding condensation, here we find that, using catalyst **1** and PPh_3

reductant, reversal of (a) and (b) is disfavoured by $23.0 \text{ kcal mol}^{-1}$ at the M06-L/SDD/6-311 + G^{**} /SMD level of theory, effectively excluding this sequence of reaction (see Figure S2 where the full DODH pathways are compared for

substrate 1,2-hexanediol). The initial loading of the substrate **S2**, via **TS1 s**, is $14.8 \text{ kcal mol}^{-1}$; this barrier is lower in energy than the barrier associated with immediate reduction of **1**, via **TS-1** (Figure S1b) which is $37.8 \text{ kcal mol}^{-1}$. Additionally, comparison of the two reduction transition states suggests that the reduction transition state in which the reduction precedes condensation is 6.7 kcal/mol higher in energy than **TS3s** in which the condensation precedes reduction. Therefore, we predict that the condensation of the substrate diol is likely to occur before the reduction of **1**.

The final phase of the mechanism is olefin extrusion. This has been the problematic stage for DODH of cyclic *trans*-diol substrates in previous computational studies using rhenium catalysts, where only one-step concerted extrusion mechanisms were considered.^[12] These mechanisms invoke an E_i *syn* elimination, which requires a co-planar arrangement of catalyst and substrate atoms that the *trans*-diol is unable to readily adopt (Figure S1). Here, however, we consider the possibility of stepwise cleavage of the diol's C–O bonds, applied to the cyclic *trans*-diol intermediate in its triplet state, **7t** (Figure 4). Firstly, step (d) involves cleavage of one diol C–O bond, forming radical **8t**. This is accompanied by the shortening of the V–O bond distance from 1.91 \AA in intermediate **7t** to 1.62 \AA in intermediate **8t**, suggesting the formation of a V=O double bond, as depicted in intermediate **8t** (Figure 4). This step passes through **TS4 t** (Figure 5a) and is rate-determining in the overall mechanism; here we find a substantial energetic barrier of $41.5 \text{ kcal mol}^{-1}$ (Figure 4). However, this activation energy is considerably lower than that computed for the rhenium-catalysed DODH of **S2** ($71.0 \text{ kcal mol}^{-1}$), with respect to MTO and **S2**, calculated at M06/SDD/6-311++G**/SMD according to the level of theory employed by Wang and co-workers.^[12] Although this estimate may vary in magnitude according to density functional and basis set, it is nevertheless expected to remain highly disfavoured due to the *trans*-diol stereochemistry.

From **TS4 t**, species **8t** is formed in the vanadium(IV) oxidation state; this oxidation state is implied by the spin density concentrated on the substrate carbon atom C_2 (1.07) and on the vanadium centre (1.14). As such, carbon C_2 is trigonal planar (for atom labelling, see Figure 2). From complex

8t, triphenylphosphine oxide is eliminated to generate **9t** (Figure 4). Next, step (e) involves a second spin-crossover to form **9s** in the singlet state (Figure 4), where the intermediate **9t** collapses to form metallacycle **9s**. The formation of the metallacycle is enabled by a rotation around the V–O₁–C₁–C₂ dihedral angle, with a value of -89.9° in **9t** (Figure 5b) to -21.6° in **9s** (Figure 5c). The rotation enables alkylation of the V centre by carbon C_2 of the *trans*-diol substrate, leading to the *syn* stereochemistry of the aliphatic C_1 and C_2 protons in **9s** (Figure 5c) required for concerted elimination in the final step (f): here, the alkyvanadium metallacycle proceeds through a [2+2] retrocycloaddition to give product **P2** (Figure 4).^[14] This concerted cleavage of C–O and C–V bonds in **TS5 s** also regenerates the starting catalyst, **1**. The **9t**–**9s** spin-crossover reaction ensures the starting catalyst is in its singlet form.

Thus, we have described here a stepwise mechanism of DODH catalysed by **1** which can process cyclic *trans*-diol **S2** leading to alkene product. We note that during our analysis of DODH of **S2**, additional pathways for extrusion of the olefin were identified. However, pathways that did not involve the triplet state of vanadium had computed energetic barrier heights of more than 50 kcal mol^{-1} (Figure S3). Also, no stationary points associated with a mechanism of concerted C–O cleavage were obtained.

In order to further probe the role of light on the reaction mechanism, we used time-dependent DFT to compute the excited states and associated absorption spectra of the first intermediate involved in intersystem crossing, *i.e.* structure **7s**, for all substrate diols studied experimentally. As **1** is not photoactive, that is, does not absorb in the visible region, it was thought that this key intermediate **7s** may have an absorption with a wavelength in the visible region. For all substrates, at the CAM–B3LYP/SDD/6-311++G**/SMD level of theory, we find that their corresponding **7s** structures exhibit strong predicted absorption in the cyan-green light region, with wavelengths ranging from 502–518 nm (Figure S4). Absorption of green light would result in a purple solution, which corresponds to the colour observed experimentally in this study (Figure S5).

Interestingly, the strongest absorption in the visible region for the **7s** singlet state appears to correspond to an excitation mainly composed of a transition from the highest occupied

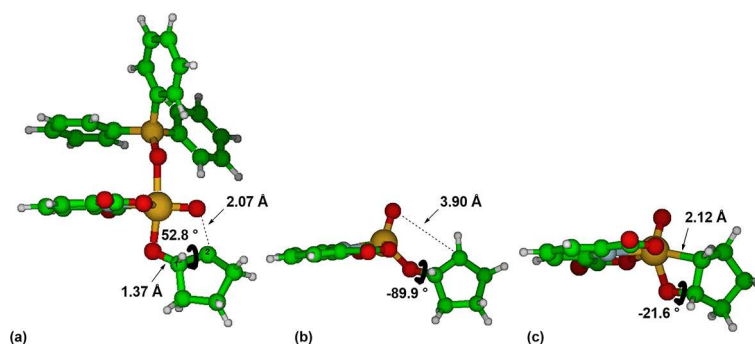


Figure 5. Optimised structures of species (a) **TS4 t**, (b) **9t** and (c) **9s** for DODH of **S2**, computed at the M06-L/SDD/6-311++G**/SMD level of theory. Bond distances in Å. Dihedral angles in ° for (a) O₁–C₁–C₂–O₂ and (b,c) V–O₁–C₁–C₂.

molecular orbital (HOMO) of **7s** to its lowest unoccupied molecular orbital (LUMO) (Figures 6 and S6; Tables S1 and S2). The HOMO has significant metal 3d character with additional contributions from the dipic ligand and to a lesser extent the substrate diol groups. The LUMO has a strong π -character and is located on the triphenylphosphine atoms. This suggests the singlet excitation has the nature of a metal-to-ligand charge transfer (MLCT). The excited singlet state then crosses to a triplet state, potentially with assistance from vibrational overlap. For the triplet ground state of **7t**, a computed spin density of 1.89 is found on the vanadium centre, the unpaired electrons occupying d-orbitals of the metal. This is prior to C–O bond cleavage and redistribution of spin density in species **8t** across the metal centre (1.14) and the reacting substrate diol carbon C₂ (1.07).

We also compute the DODH pathway for corresponding *cis*-isomer of **S2**, namely **S2'** (Table 1, Figure S7). For substrate **S2'**, the transition state for the reduction by triphenylphosphine, **TS3 s'**, is 6.3 kcal mol⁻¹ lower than for **S2** (Figure S7). The minimum energy crossing point for the transition of **7s'** to **7t'** is also more facile for this *cis*-diol substrate, by 6.4 kcal mol⁻¹. Interestingly, however, the transition state for C–O cleavage prior to elimination of triphenylphosphine oxide, **TS4 t'**, could not be located. Instead, we find a route where triphenylphosphine oxide leaves before C–O scission, through transition state **TS6 t'** to form radical intermediate **9 t'**. The computed relative free energy for **TS6 t'** is 30.7 kcal mol⁻¹ (Figure S7); this is 12.8 kcal mol⁻¹ more stable than for the equivalent of its isomeric **TS6 t** of *trans*-diol **S2** (Figure S4) where the *trans*-diol displays a non-ideal geometry.

In addition we note that a low-lying singlet pathway to DODH is available to **S2'**, via transition state **TS8 s'**, with a calculated free-energy barrier of 30.5 kcal mol⁻¹, similar to that of **TS6 t'** (Figure S7). This extrusion route involves concerted C–O cleavage due to a *syn* orientation of the *cis*-diol moiety. Thus, both singlet and triplet pathways are predicted to coexist for cyclic *cis*-diol **S2'**. Overall, for singlet and triplet pathways, the rate-determining step is the reduction via **TS3 s'**, with a barrier of 34.0 kcal mol⁻¹. Experimentally, we find similar yields

for both **S2** and **S2'** isomers at the elevated temperature of 170 °C for 72 h. The disparity in the rate-determining steps in the reaction pathways of **S2**, via **TS4 t** at 41.5 kcal mol⁻¹ and **S2'** through **TS3 s** at 34.0 kcal mol⁻¹ would suggest that potentially additional unexplored pathways could be available to the cyclic *trans*-diol.

We briefly also consider the computed reaction pathways of *cis* and *trans* isomers of 1,4-anhydroerythritol, namely **S1'** and **S1** (Figure S1a). These are analogues of **S2** and **S2'** and allow consideration of the effect of including an oxygen in the ring. Here, unsurprisingly, we find *trans*-diol substrate **S1** follows a pathway analogous to **S2**, with stepwise cleavage of the diol C–O bonds via the triplet state (Figure S8). Indeed, the computed energies for the corresponding transition state **TS4 t** differ by only 2.7 kcal mol⁻¹ between **S1** and **S2**. As for **S2**, no concerted routes to extrusion are accessible. The reduction step via **TS3 s** is rate-determining for **S1**, with a relative energy of 39.8 kcal mol⁻¹, very similar to a value of 40.3 kcal mol⁻¹ for the equivalent **TS3 s** structure of **S2** (Figure 3).

By contrast, *cis*-diol **S1'**, is predicted to have accessible concerted as well as stepwise pathways for extrusion (Figure S9). As for **S2'**, the concerted routes are via the singlet state (**TS7 s'** and **TS8 s'**, Figure S9); and the stepwise pathway is through the triplet state (**TS6 t'**), where the first diol C–O bond is cleaved after elimination of triphenylphosphine oxide. Both concerted transition states **TS7 s'** and **TS8 s'** satisfy the requirement for *syn* co-planar arrangement in E_i elimination with O₁–C₁–C₂–O₂ dihedral angles of 6.1 and 4.8°, respectively. The energy barriers associated with the stepwise and concerted transition states are similar, ranging from 31.2–32.6 kcal mol⁻¹, and constitute the rate-determining step.

Overall, the highest barriers for the DODH pathways of **S1** and **S1'** are similar in free energy to those of their respective **S2** and **S2'** analogues, differing at most by 2.7 kcal mol⁻¹ for the *trans* substrates and 4.3 kcal mol⁻¹ for the *cis* reactants. This suggests only a moderate effect on energetics by the presence of a ring oxygen in the substrate. Of significant note, for cyclic *trans*-diol **S1**, the energy barrier for its V-catalysed rate-determining step is 39.8 kcal mol⁻¹ (**TS3 s**, Figure S8); this is over 30 kcal mol⁻¹ lower in energy than the rate-determining step calculated previously for the DODH of **S1** via the rhenium catalyst MTO.^[12] Although the latter calculation differs in using the M06 rather than M06-L functional employed here, the difference in computed barrier height is substantial.

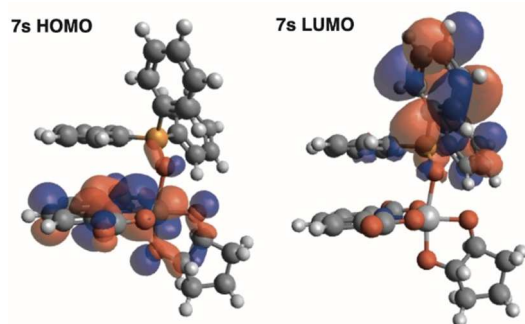


Figure 6. Key molecular orbitals involved in proposed transition of intermediate **7s** from ground-state singlet to the excited singlet (**7s** HOMO to LUMO). Calculations performed at the CAM–B3LYP/SDD/6-311 + G**/SMD level of theory (although we note similar orbital features were obtained via M06-L/SDD/6-311 + G**/SMD level).

Linear substrate

An interesting comparison for the DODH profiles of constrained cyclic diols is with that of a linear acyclic substrate, where the latter's diol moiety can in principle orient optimally with the catalyst. For this, we consider the commonly studied DODH substrate, 1-phenyl-1,2-ethanediol **S4** (Table 1). For **S4**, we find that concerted singlet pathways (via **TS7 s** and **TS8 s**) and stepwise pathways involving the triplet state (through **TS4 t** and **TS6 t**) are predicted as feasible mechanisms of DODH (Figure 7). For the stepwise routes of **S4**, these energy barriers

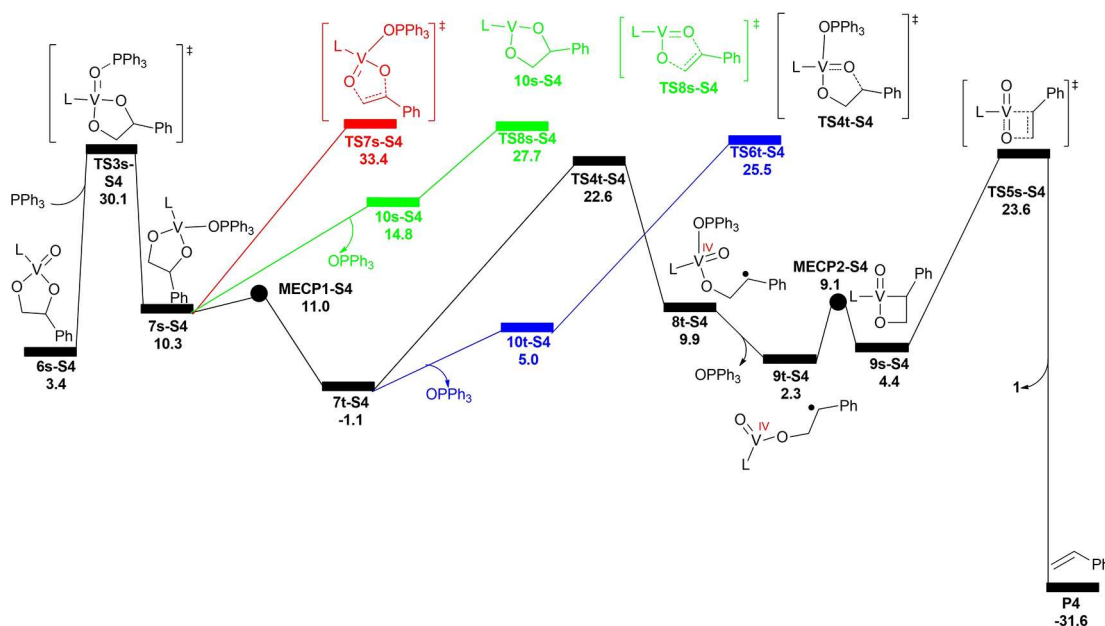


Figure 7. DODH reaction pathway for 1-phenyl-1,2-ethanediol (S4). Free energies [kcal mol⁻¹] computed at the M06-L/SDD/6-311 + G**/SMD level of theory.

are 2.2 to 10.8 kcal mol⁻¹ lower than for its concerted pathways. The rate-determining step is reduction, with an energy barrier for **TS3 s** of 30.1 kcal mol⁻¹, more similar to that of *cis*-diol **S2'** (34.0 kcal mol⁻¹) than *trans*-diol **S2** (40.3 kcal mol⁻¹).

Indeed, both the reduction and extrusion barriers of **S4** were the lowest calculated of all substrates considered in our study, with energy values of 30.1 and 22.6 kcal mol⁻¹, respectively (Figure 7). Correspondingly, **S4** had the highest olefin yield of all the substrates observed experimentally, of 36% in visible light and 14% in its absence (Table 1). Nevertheless, comparison of the **TS4 t** geometries for the DODH reaction of **S4** compared to *trans*-diol substrate **S2** shows similarities in bond angles and distances (Figure S10): in the fully flexible linear substrate **S4**, the orientation of the diol carbons C₁ and C₂ gives a O₁-C₁-C₂-O₂ torsion angle value of 45.1° (Figure S10b), similar to a value of 52.8° in the *trans*-cyclic diol **S2** (Figure 5a). Likewise, the C₂...O₂=V distance is 1.99 Å in **S4** and 2.07 Å in **S2** (Figure S10). This similarity suggests that the *trans* stereochemistry of the aliphatic CH protons in **S2** is compatible with a productive presentation of the diol O₂ oxygen to the V centre of the DODH catalyst.

Six-membered ring substrates

Our observation that [n-Bu₄N]-(dipic)VO₂ can catalyse the DODH of both five and six-membered ring *trans* diols experimentally (Table 1) is encouraging for the potential processing of carbohydrate compounds. As an indication of the feasibility of processing *trans*-diol hexapyranose saccharides, we compute the DODH reduction and extrusion steps for sugar analogues *trans*- and *cis*-1,5-anhydro-2-deoxypentitol **S5** and **S5'** respectively (Figures S11 and S12). As for other *trans*-diol substrates

S1 and **S2**, the six-membered pyranose **S5** can proceed through a stepwise extrusion DODH mechanism via the triplet state (Figure S11). Interestingly, the extrusion step through **TS4 t** is significantly more favoured for **S5** than five-membered ring substrates, with energy barriers lower than for the corresponding **S1** and **S2** structures by 8.9 and 11.6 kcal mol⁻¹, respectively; and for extrusion via the **TS6 t** transition state, energy barriers lower by 16.5 and 16.3 kcal mol⁻¹, respectively. Interestingly, a singlet route for stepwise extrusion is also possible for the more flexible six-membered ring system of **S5**: the transition state **TS6 s** is lowered in energy from 49.1 kcal mol⁻¹ for **S1** to 28.6 kcal mol⁻¹ for **S5**. While stepwise singlet and triplet pathways are accessible to **S5**, no concerted pathway is found, as for other the *trans*-diol substrates we considered. The rate-determining step for DODH is predicted to be the reduction: transition state **TS3 s** has a computed relative free energy of 31.7 kcal mol⁻¹ (Figure S11), which is also reduced compared to the strained rings of **S1** (39.8 kcal mol⁻¹, Figure S8) and **S2** (40.3 kcal mol⁻¹, Figure 3).

The six-membered ring *cis*-diol **S5'** is able to proceed through a concerted route, with a barrier of 33.2 kcal mol⁻¹ via transition state **TS8 s'** (Figure S12). Interestingly, **S5'** is also able to follow a stepwise spin-crossover mechanism such that **TS4 t'** could be located, representing a barrier of 23.2 kcal mol⁻¹ for formation of intermediate **8 t'** (Figure S12). This suggests that the additional degrees of freedom of the tetrahydropyran ring facilitate the geometry required for formation of **TS4 t'**, in contrast to five-membered ring substrates such as **S1'** and **S2'**. Indeed, substrate **S5'** possesses a O₁-C₁-C₂-O₂ dihedral angle of -30.6° in intermediate **7 t'**, in contrast to the almost coplanar arrangement of -2.2° for the **7 t'** intermediate of substrate **S1'**. Correspondingly, substrate **S5'** and catalyst **1** can suitably orientate for elimination, forming a O₁-C₁-C₂-O₂

torsion angle of 42.5° in **TS4 t'**. The rate-determining step for DODH of **S5'** is the reduction, with an energetic barrier of $32.1 \text{ kcal mol}^{-1}$ through **TS3 s'**. In this case, the barrier is slightly higher than that found for the other cyclic *cis*-diols, for example $30.7 \text{ kcal mol}^{-1}$ for **TS3 s'** of **S1'** (Figure S9). The difference between the rate-determining step through **TS3 s** for **S5** and **S5'** is $0.4 \text{ kcal mol}^{-1}$. Therefore, it is unsurprising that for model substrates *cis*- and *trans*-1,2-cyclohexanediol, we observe comparable yields experimentally where we obtain 14% of cyclohexene from the DODH reaction of the *trans* isomer in comparison to 16% for the *cis* form (Table 1).

Conclusions

The feasibility of the vanadium-catalysed DODH reaction of cyclic *trans*-diols has been demonstrated experimentally and explored computationally. Here, we show that direct DODH of cyclic *trans*-diols can occur in the presence of catalyst, $[n\text{-Bu}_4\text{N}]\text{-(dipic)VO}_2$ and triphenylphosphine reductant. Furthermore, for the five substrates considered here, product yield shows a dependence on light. This observation suggests the involvement of the triplet state of vanadium in the DODH mechanism involving these substrates, although the generality of this finding to a wider range of diol substrates remains to be established. Computational study of the mechanism proposes a two-step olefin extrusion for the five-membered ring *trans*-diol substrates **S1** and **S2** via the triplet state; for the six-membered ring **S5** *trans*-diol, in addition to this pathway, a stepwise route on the singlet surface is also predicted as possible. For *cis*-diols **S1'**, **S2'** and **S5'** and linear substrate **S4**, concerted pathways on the singlet surface are identified as well as stepwise routes via intersystem crossing. We note that the computed rate-determining free energy barrier for the DODH of six-membered ring **S5** *trans*-diol is $31.7 \text{ kcal mol}^{-1}$; for the five-membered *trans*-diol substrates **S1** and **S2**, these barriers are 39.8 and $41.5 \text{ kcal mol}^{-1}$ respectively. While this is consistent with the observation that DODH of *trans*-diols is not a very efficient reaction, the calculated estimates for **S1** and **S2** are at the limit of what is acceptable for the generation of alkenes under the reported experimental conditions ($150\text{--}170^\circ\text{C}$, $24\text{--}72 \text{ h}$). The rate-determining energetic barriers calculated here for stepwise DODH of **S1** and **S2** correspond to estimated rates of approximately 10^{-8} s^{-1} at the elevated temperatures required for the reaction. This may point to the potential existence of additional DODH routes for these five-membered ring systems. Nevertheless, in this work we have demonstrated the feasibility of DODH of five- and six-membered cyclic *trans*-diol substrates using V catalysis. In particular, the ability of this vanadium-based DODH catalyst to process six-membered *trans*-diol compounds suggests that further optimisation of its efficiency could provide a new cost-effective route to converting biomass-derived substrate diols such as glucose into high-value alkenes.

Experimental Section

All reagents were purchased from Sigma Aldrich and used without further purification. DODH reactions were repeated three times and average yields are reported here. We describe here the general DODH reaction set up: under N_2 , the substrate diol (0.1 mmol), PPh_3 (0.15 mmol), $[n\text{-Bu}_4\text{N}]\text{-(dipic)VO}_2$ (0.01 mmol) and chlorobenzene (0.5 mL) were combined in a thick-walled ace pressure tube, equipped with a stirrer bar. The sealed tube was placed in a preheated oil bath (temperature 170°C) and the reaction was left to stir for $24\text{--}72 \text{ h}$. The reaction was cooled in an ice bath and the internal standard mesitylene ($18 \mu\text{L}$, 0.13 mmol) was added and the reaction was stirred. A small aliquot was taken and diluted with CDCl_3 and the yield was determined by $^1\text{H NMR}$ spectroscopy. $[n\text{-Bu}_4\text{N}]\text{-(dipic)VO}_2$ **1** was synthesised from $[n\text{-Bu}_4\text{N}]\text{VO}_3$ according to the procedure reported by Chapman and Nicholas.^[8a] $[n\text{-Bu}_4\text{N}]\text{VO}_3$ was synthesised according to the procedure of Day et al.^[16]

Computational methods

All density functional calculations were performed using the Gaussian 09 electronic structure package.^[17] We use the Minnesota suite of functionals: specifically, energy and geometry calculations employed the M06-L functional,^[18] suited to computing thermodynamics of transition metal systems.^[19] For example, the M06-L functional was found to perform well in the challenging task of predicting the ground spin states of Fe^{II} , Fe^{III} and Fe^{IV} systems.^[20] An SDD effective core potential^[21] was employed on V and a 6-311 + G** basis on all other atoms. Solvent was modelled using the SMD solvation model of benzene.^[22] We note that this level of theory reproduces well the bond distances of the crystallographic structure of $[(\text{dipic})\text{VO}_2]^-$ anion, with an average deviation in bond distance of 0.01 \AA (Table S3). The largest differences are for V–O distances, which are predicted to within 0.05 \AA ; this arises from the involvement of these oxygen atoms in a hydrogen-bonding interaction with neighbouring ammonium counterions in the crystal structure.^[23]

Stationary points were characterised as minima or transition states by calculation of vibrational frequencies and intrinsic reaction coordinate (IRC) analyses. Thermal corrections for free energies were carried out at 298.15 K and 1 atm using harmonic frequencies obtained above. Restricted and unrestricted DFT calculations were used for singlet and triplet states, respectively. The wavefunctions for all stationary points on the reaction pathway of *trans*-1,2-cyclopentanediol were tested and confirmed as stable. Minimum energy crossing points (MECP) between singlet and triplet states were calculated using the program developed by Harvey et al.^[24] Excited state calculations using time-dependent DFT were carried out, solving for the first twelve low-lying excited states. This was performed using the CAM-B3LYP functional^[25] employing the SDD pseudopotential for vanadium atoms and 6-311 + G** for all other atoms. The solvent was modelled via SMD model for benzene. These were performed using geometries obtained at the M06-L/SDD/6-311 + G**/SMD level of theory.

Supporting information

The Supporting Information includes computed reaction schemes, energetics, geometries, molecular orbitals, predicted excitations and UV/Vis spectra, as well as further experimental details.

Acknowledgements

This work was supported by The University of Manchester and A*STAR Institute of Chemical and Engineering Sciences (ICES). E.A. acknowledges support from A*STAR Graduate Academy through the ARAP program. The authors also thank Drs Mark Vincent and Irfan Alibay for support in running and analysing DFT calculations, and Drs. Charles W. Johannes and Kok Ping Chan for initial insightful discussions; and The University of Manchester's Research IT for their assistance and use of the Computational Shared Facility.

Conflict of Interest

The authors declare no conflict of interest.

Keywords: biomass conversion · density functional calculations · deoxydehydration · sustainable chemistry · vanadium

- [1] L. J. Donnelly, S. P. Thomas, J. B. Love, *Chem. Asian J.* **2019**, *14*, 3782–3790.
- [2] N. N. Tshibalonza, J.-C. M. Monbaliu, *Green Chem.* **2020**, *22*, 4801–4848.
- [3] a) K. A. DeNike, S. M. Kilyanek, *R. Soc. Open Sci.* **2019**, *6*, 191165; b) J. R. Dethlefsen, P. Fristrup, *ChemSusChem* **2015**, *8*, 767–775.
- [4] S. Raju, M.-E. Moret, R. J. M. K. Gebbink, *ACS Catal.* **2015**, *5*, 281–300.
- [5] S. Dutta, *ChemSusChem* **2012**, *5*, 2125–2127.
- [6] J. O. Metzger, *ChemCatChem* **2013**, *5*, 680–682.
- [7] a) G. K. Cook, M. A. Andrews, *J. Am. Chem. Soc.* **1996**, *118*, 9448–9449; b) J. E. Ziegler, M. J. Zdilla, A. J. Evans, M. M. Abu-Omar, *Inorg. Chem.* **2009**, *48*, 9998–10000; c) E. Arceo, J. A. Ellman, R. G. Bergman, *J. Am. Chem. Soc.* **2010**, *132*, 11408–11409; d) S. Vkuturi, G. Chapman, I. Ahmad, K. M. Nicholas, *Inorg. Chem.* **2010**, *49*, 4744–4746; e) J. Yi, S. Liu, M. M. Abu-Omar, *ChemSusChem* **2012**, *5*, 1401–1404; f) M. Shiramizu, F. D. Toste, *Angew. Chem. Int. Ed.* **2012**, *51*, 8082–8086; *Angew. Chem.* **2012**, *124*, 8206–8210; g) M. Shiramizu, F. D. Toste, *Angew. Chem. Int. Ed.* **2013**, *52*, 12905–12909; *Angew. Chem.* **2013**, *125*, 13143–13147; h) A. L. Denning, H. Dang, Z. Liu, K. M. Nicholas, F. C. Jentoft, *ChemCatChem* **2013**, *5*, 3567–3570; i) C. Boucher-Jacobs, K. M. Nicholas, *ChemSusChem* **2013**, *6*, 597–599; j) P. Liu, K. M. Nicholas, *Organometallics* **2013**, *32*, 1821–1831; k) S. Raju, J. Jastrzebski, T. B. H. M. Lutz, R. J. M. Klein Gebbink, *ChemSusChem* **2013**, *6*, 1673–1680; l) I. McClain, J. Michael, K. M. Nicholas, *ACS Catal.* **2014**, *4*, 2109–2112; m) X. Li, D. Wu, T. Lu, G. G. Yi, H. Su, Y. Zhang, *Angew. Chem. Int. Ed.* **2014**, *53*, 4200–4204; *Angew. Chem.* **2014**, *126*, 4284–4288; n) N. Ota, M. Tamura, Y. Nakagawa, K. Okumara, K. Tomishige, *ACS Catal.* **2016**, *6*, 3213–3226; o) D. S. Morris, K. van Rees, M. Curcio, M. Cokoja, F. E. Kuhn, F. Duarte, J. B. Love, *Catal. Sci. Technol.* **2017**, *7*, 5644–5649; p) N. Shin, S. Kwon, S. Moon, C. H. Hong, Y. G. Kim, *Tetrahedron* **2017**, *73*, 4758–4765; q) J. H. Jang, H. Sohn, J. Camacho-Bunquin, D. Yang, C. Y. Park, M. Delferro, M. M. Abu-Omar, *ACS Sustainable Chem. Eng.* **2019**, *7*, 11438–11447; r) M. Lupacchini, A. Mascitti, V. Canale, L. Tonucci, E. Colacino, M. Passacantando, A. Marrone, N. d'Alessandro, *Catal. Sci. Technol.* **2019**, *9*, 3036–3046; s) S. Raju, C. A. M. R. van Slagmaat, T. B. H. M. Lutz, J. Jastrzebski, E. Moret, R. J. M. Klein Gebbink, *Organometallics* **2016**, *35*, 2178–2187; t) J. Li, M. Lutz, M. Otte, R. J. M. Klein Gebbink, *ChemCatChem* **2018**, *10*, 4755–4760.
- [8] a) G. Chapman Jr, K. M. Nicholas, *Chem. Commun.* **2013**, *49*, 8199–8201; b) T. V. Gopaladasu, K. M. Nicholas, *ACS Catal.* **2016**, *6*, 1901–1904; c) K. M. Kwok, C. K. S. Choong, D. S. W. Ong, J. C. Q. Ng, C. G. Gwie, L. Chen, A. Borgna, *ChemCatChem* **2017**, *9*, 2443–2447; d) A. R. Petersen, L. B. Nielsen, J. R. Dethlefsen, P. Fristrup, *ChemCatChem* **2018**, *10*, 769–778.
- [9] a) J. R. Dethlefsen, D. Lupp, B.-C. Oh, P. Fristrup, *ChemSusChem* **2014**, *7*, 425–428; b) J. R. Dethlefsen, D. Lupp, A. Teshome, L. B. Nielsen, P. Fristrup, *ACS Catal.* **2015**, *5*, 3638–3647; c) D. Lupp, N. J. Christensen, J. R. Dethlefsen, P. Fristrup, *Chem. Eur. J.* **2015**, *21*, 3435–3442; d) K. Beckerle, A. Sauer, T. P. Spaniol, J. Okuda, *Polyhedron* **2016**, *116*, 105–110; e) L. Sandbrink, K. Beckerle, I. Meiners, R. Liffmann, K. Rahimi, J. Okuda, R. Palkovits, *ChemSusChem* **2017**, *10*, 1375–1379; f) B. E. Sharkey, A. L. Denning, F. C. Jentoft, R. Gangadhara, T. V. Gopaladasu, K. M. Nicholas, *Catal. Today* **2018**, *310*, 86–93; g) M. Stalpaert, K. De Vos, *ACS Sustainable Chem. Eng.* **2018**, *6*, 12197–12204; h) R. Tran, S. M. Kilyanek, *Dalton Trans.* **2019**, *48*, 16304–16311; i) A. R. Petersen, P. Fristrup, *Chem. Eur. J.* **2017**, *23*, 10235–10243; j) L. Hills, R. Moyano, F. Montilla, A. Pastor, A. Galindo, E. Alvarez, F. Marchetti, C. Pettinari, *Eur. J. Inorg. Chem.* **2013**, 3352–3361.
- [10] I. Ahmad, G. Chapman, K. M. Nicholas, *Organometallics* **2011**, *30*, 2810–2818.
- [11] a) V. Canale, L. Tonucci, M. Bressan, N. d'Alessandro, *Catal. Sci. Technol.* **2014**, *4*, 3697–3704; b) A. Jefferson, R. S. Srivastava, *Polyhedron* **2019**, *160*, 268–271.
- [12] S. Qu, Y. Dang, M. Wen, Z.-X. Wang, *Chem. Eur. J.* **2013**, *19*, 3827–3832.
- [13] Y.-Y. Jiang, J.-L. Jiang, Y. Fu, *Organometallics* **2016**, *35*, 3388–3396.
- [14] L. C. d. V. Poutas, M. C. Reis, R. Sanz, C. S. Lopez, O. N. Faza, *Inorg. Chem.* **2016**, *55*, 11372–11382.
- [15] A. Galindo, *Inorg. Chem.* **2016**, *55*, 2284–2289.
- [16] V. W. Day, W. G. Klemperer, A. Yagasaki, *Chem. Lett.* **1990**, *19*, 1267–1270.
- [17] M. J. Frisch, G. W. Trucks, H. B. Schlegel, G. E. Scuseria, M. A. Robb, J. R. Cheeseman, G. Scalmani, V. Barone, G. A. Petersson, H. Nakatsuji, X. Li, M. Caricato, A. Marenich, J. Bloino, B. G. Janesko, R. Gomperts, B. Mennucci, H. P. Hratchian, J. V. Ortiz, A. F. Izmaylov, J. L. Sonnenberg, D. Williams-Young, F. Ding, F. Lipparini, F. Egidi, J. Goings, B. Peng, A. Petrone, T. Henderson, D. Ranasinghe, V. G. Zakrzewski, J. Gao, N. Rega, G. Zheng, W. Liang, M. Hada, M. Ehara, K. Toyota, R. Fukuda, J. Hasegawa, M. Ishida, T. Nakajima, Y. Honda, O. Kitao, H. Nakai, T. Vreven, K. Throssell, J. A. J. Montgomery, J. E. Peralta, F. Ogliaro, M. Bearpark, J. J. Heyd, E. Brothers, K. N. Kudin, V. N. Staroverov, T. Keith, R. Kobayashi, J. Normand, K. Raghavachari, A. Rendell, J. C. Burant, S. S. Iyengar, J. Tomasi, M. Cossi, J. M. Millam, M. Klene, C. Adamo, R. Cammi, J. W. Ochterski, R. L. Martin, K. Morokuma, O. Farkas, J. B. Foresman, D. J. Fox, *Revision D.01 Ed.*, Gaussian Inc., Wallingford CT, **2013**.
- [18] Y. Zhao, D. G. Truhlar, *J. Chem. Phys.* **2006**, *125*, 194101.
- [19] a) B. S. Narendrapurapu, N. A. Richardson, A. V. Copan, M. L. Estep, Z. Yang, H. F. Schaefer, *J. Chem. Theory Comput.* **2013**, *9*, 2930–2938; b) C. J. Cramer, D. G. Truhlar, *Phys. Chem. Chem. Phys.* **2009**, *11*, 10757–10816.
- [20] P. Verma, Z. Varga, J. E. M. N. Klein, C. J. Cramer, L. Que, D. G. Truhlar, *Phys. Chem. Chem. Phys.* **2017**, *19*, 13049–13069.
- [21] a) D. Andrae, U. Haussermann, M. Dolg, H. Stoll, H. Preuss, *Theor. Chim. Acta* **1990**, *77*, 123–141; b) G. Igel-Mann, H. Stoll, P. Preuss, *Mol. Phys.* **1988**, *65*, 1321–1328.
- [22] A. V. Marenich, C. J. Cramer, D. G. Truhlar, *J. Phys. Chem. B* **2009**, *113*, 6378–6396.
- [23] B. S. Parajon-Costa, O. E. Piro, R. Pis-Diez, E. E. Castellano, A. C. Gonzalez-Baro, *Polyhedron* **2006**, *25*, 2920–2928.
- [24] J. N. Harvey, M. Aschi, H. Schwarz, W. Koch, *Theor. Chem. Acc.* **1998**, *99*, 95–99.
- [25] T. Yanai, D. P. Tew, N. C. Handy, *Chem. Phys. Lett.* **2004**, *393*, 51–57.

Manuscript received: November 6, 2020
 Revised manuscript received: January 11, 2021
 Accepted manuscript online: January 19, 2021
 Version of record online: February 9, 2021